IUP Multiyear Ice Concentration and other sea ice types,

Version 1.1 (Arctic)/Version AQ2 (Antarctic)

User Guide

Institute of Environmental Physics, University of Bremen

Christian Melsheimer, Gunnar Spreen

Version V1.08 (November 16, 2022)

Contents

1 Introduction

This document is intended for users of the multiyear ice (MYI) concentration product and the intermediate ice type product, provided by the University of Bremen, Institute of Environmental Physics (IUP), available at https:seaice.uni-bremen.de. These data are the result of the project SITAnt, grant SP1128/2-1, by the Deutsche Forschungsgemeinschaft (DFG) in the framework of the Antarctic priority programme SPP 1158 "Antarctic Research with comparative investigations in Arctic ice areas".
The multiyear ice (MYI) concentration data are retrieved in a two-step procedure using first the Environment Canada Ice Concentration Extractor (ECICE) system (Shokr et al., 2008; Shokr and Agnew, 2013) and several correction schemes by Ye et al. (2016a,b). These correction schemes correct misclassifications by ECICE caused by melt and refreezing and by snow metamorphosis.
The implementation of ECICE at the IUP uses as input microwave radiometer data of the sensors AMSR-E (Advanced Microwave Scanning Radiometer for EOS) on the NASA satellite Aqua, or AMSR2 (Advanced Microwave Scanning Radiometer 2) on the JAXA satellite GCOM-W1, and scatterometer data from ASCAT (Advanced Scatterometer) on the European polar-orbiting satellites MetOp-A and MetOp-B. The correction schemes in addition use surface temperature data from meteorological reanalysis of the European Centre for Medium-Range Weather Forecast (ECMWF), namely, from the ERA Interim data set, and sea ice motion data from the Satellite Application Facility on Ocean and Sea Ice (OSISAF) or from the National Snow and Ice Data Center (NSIDC).
The final result of the two-step retrieval are MYI data. In addition, as an intermediate result, a preliminary distinction of the sea ice into three types, i.e., MYI, first-year ice (FYI) and young ice (YI) is produced as well.
As the algorithms for the Arctic and for the Antarctic use different calibrations and tuning parameters, different versions of the retrieval are used for the Arctic and the Antarctic. The current version for the Arctic is *Version 1.1*. To avoid confusion, the version number for the Antarctic is prefixed with "AQ" (top level domain name for Antarctica), the current one is *version AQ2*. The details are explained in the following sections.

2 Input Data

2.1 Microwave Radiometer

Details about the input data from the two sensors AMSR-E and AMSR2 are specified in Table 1

Sensor	Data	Lvl	Version	Time Range	Source
AMSR-E	raw obs. counts	1A	3	2002-06-01 - 2011-10-04	NASA/JAXA[a]
AMSR2	brightness temp.	1B	2.220.220	2 Jul 2012 – today	JAXA[b]

[a] JAXA (2003)
[b] JAXA G-Portal, https://gportal.jaxa.jp

Table 1: *Input microwave radiometer data for ECICE. Note: Lvl = Processing Level, obs. = observation, temp. = temperature.*

Both sensors measure the brightness temperature (i.e., microwave radiance) at several frequency channels at both horizontal (H) and vertical (V) polarisation. The frequency channels relevant here are 18.7 and 36.5 GHz (short version: 19 and 37 GHz).

The input data come as two files per orbit (i.e., two half-orbits) and contain the measured values in all channels for each satellite footprint and the geographical location of each footprint – this is called swath data, see details about reading the swath data in the appendix, Section A. The half-orbits are either descending or ascending. There are about 29 to 30 half-orbit swath files per day. The instrument is conically scanning at constant looking angle, therefore, the scan lines are circle segments. For the channels used here, i.e., at 19 and 37 GHz, the spacing between successive footprints in one scan line is 10 km, and the spacing between successive scan lines is 10 km in flight direction. The size of the individual footprints, however, is about 7×12 km at 37 GHz and 14×22 km at 19 GHz. For the input into the MYI concentration retrieval, data from all swaths of one day are combined and interpolated to polar stereographic grids with nominal grid spacing of 12.5 km, see details below, Section 3.4.

2.2 Scatterometer

The ASCAT instrument on the satellites MetOp-A, -B, and -C measures the normalised radar backscattering cross section (NRCS) at C band (5.3 GHz), vertical polarisation, at three different azimuth directions to both sides. As the two swaths (one on each side) are about 550 km wide, there is considerable incidence angle variation. The data are therefore normalised to 40° incidence angle[1]. All swaths of one calendar day are resampled to the polar stereographic grids already mentioned. Until the end of of the season 2015/2016, i.e., May 2016, we use data where the conversion and resampling was done at Ifremer (Institut français de recherche pour l'exploitation de la mer)/CERSAT (Centre de Recherche et d'Exploitation Satellitaire)[2], based on ASCAT data from MetOp-A alone. After that, the ASCAT data have been converted and resampled in-house (at the IUP), based on level 1B full resolution data (sampling interval a few km) from both MetOp-A and MetOp-B. The data are resampled to the same grid as the radiometer data.

2.3 Surface Temperature

For the correction schemes (details see Section 3.3.1), 2-metre air temperatures are needed. For reprocessed complete years, we use the 2-metre air temperature (T2m) of the ERA Interim reanalysis data set of the ECMWF. For retrieval during the running season, usually only lagging about 2 weeks behind the actual date, we use the 2-metre air temperature (T2m) of the ECMWF operational analysis data. In both cases, the maximum of the four daily time steps is used. The data, originally on a 1.5° grid, are also regridded to the standard polar-stereographic grids for the Arctic and Antarctic.

2.4 Sea Ice Motion (Drift)

Additionally, one of the correction schemes (details see Section 3.3.2) needs to estimate the sea ice drift between one day and the next. We use the low resolution ice motion vectors provided by OSISAF (Lavergne et al., 2010), https://osi-saf.eumetsat.int/products/osi-405-c (product ID OSI-405-c). As this data set starts in December 2009, before that, sea ice motion data from NSIDC are used (Tschudi et al., 2016). These data are also regridded to the standard polar-stereographic grids for the Arctic and Antarctic.

[1] Using an empirical linear model for the incidence angle dependence of the NRCS for sea ice

[2] Arctic: http://products.cersat.fr/details/?id=CER_PSI_ARC_1D_012_PSI_ASCAT, Antarctic: http://products.cersat.fr/details/?id=CER_PSI_ANT_1D_012_PSI_ASCAT

3 Processing Chain

The main steps of the MYI processing chain are the following (details are described in Section 3.1 to Section 3.3.2):

- Reading regridded AMSR-E or AMSR2 brightness temperature data as well as regridded ASCAT backscattering cross section data
- Applying ECICE to the input data, resulting in the concentration of MYI, first-year ice (FYI), and young ice (YI). They are saved as NetCDF data and as maps in image format, and are called *uncorrected ice types*; they are considered an intermediate product of this processing chain.
- Applying the so-called temperature correction that mainly corrects for MYI that is episodically misclassified as FYI when there is temporary warming to near-freezing temperatures
- Applying the so-called drift correction that eliminates erroneously classified MYI (which actually can only be YI or MYI) which is too far away from the previous day's MYI to have drifted there. The resulting MYI concentration is saved as NetCDF and as maps in image format and is called *Corrected MYI concentration*. It is considered the final product of this processing chain

3.1 ECICE algorithm

The ECICE algorithm (Shokr et al., 2008; Shokr and Agnew, 2013) can use several channels of radiometer measurements (brightness temperatures) and scatterometer measurements (normalised radar backscatter cross sections) as input and can in principle distinguish as many surface types as input channels. One of the surface types is open water. Since we want to retrieve three ice types, we therefore need four input channels. Note that under melting conditions, the surface properties of all ice types change drastically and become similar. Therefore, ECICE works only during the freezing season, from autumn to spring.
The following is a brief summary of ECICE and how it is used in the retrieval chain of sea ice types at IUP, for details please refer to the references just mentioned.
Here we use the following four input channels:

σ^0 : normalised radar backscattering cross section at C band, i.e., 5.3 GHz, at 40° incidence angle (from ASCAT)

$T_{B,37V}$: brightness temperature at 36.5 GHz, vertical polarisation (from AMSR-E or AMSR2)

$T_{B,37H}$: brightness temperature at 36.5 GHz, horizontal polarisation (from AMSR-E or AMSR2)

$GR_{37V,19V}$: gradient ratio of 36.5 GHz and 18.7 GHz, vertical polarisation (from AMSR-E or AMSR2), defined as

$$GR_{37V,19V} = \frac{T_{B,37V} - T_{B,19V}}{T_{B,37V} + T_{B,19V}} \tag{1}$$

For each of the input channels, ECICE needs a distribution of typical values for each surface type. These distributions have been derived analysing areas of known ice type. Here we use the following ice types:

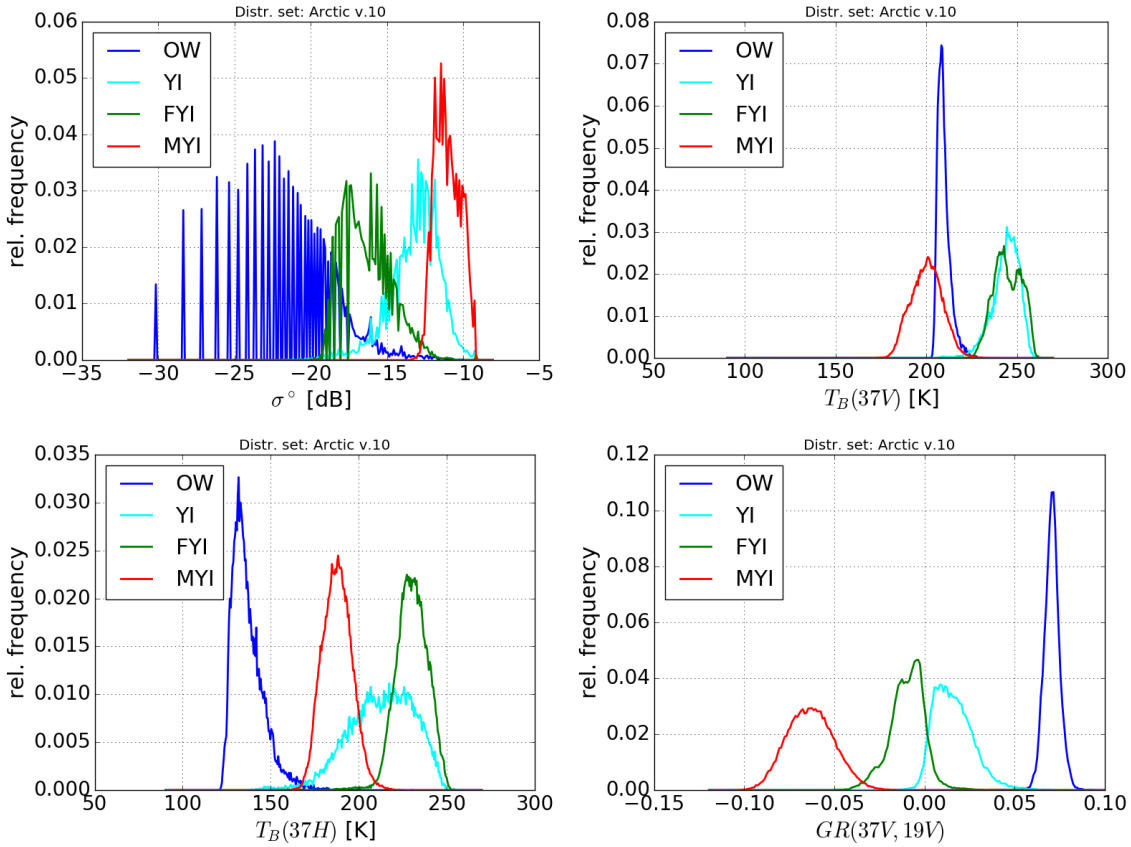

Figure 1: *Distribution of ASCAT σ^0 (top left), AMSR2 T_B at 36.5* GHz*, V polarisation (top right); AMSR2 T_B at 36.5* GHz*, H polarisation (bottom left), and AMSR2 GR(37V,19V) (bottom right) for three* ***Arctic*** *sea ice types MYI (red), FYI (green), YI (light blue) and for open water (blue).*

young ice (YI) : thin (up to 30 cm thick) new ice; includes a few sub-types; can be smooth or rough

first-year ice (FYI) : formed during one cold season; thickness above 30 cm; surface can be level, rough or with ridges

multiyear ice (MYI) : ice that has survived at least one melt season; less saline and often rougher than FYI, but topographic features are generally smoother than FYI

As the ice types, in spite of having the same names, are different for the Arctic and Antarctic, the distributions had to be derived separately for both hemispheres. The ones used for the Arctic form the set *version 1.1*, shown in Figure 1, and the ones used for the Antarctic form the set *version AQ2*, shown in Figure 2.

Based on the distributions, interpreted as probability density functions, a number n of possible realisations of typical brightness temperatures and NRCS for the four surface types (three ice types and open water) is randomly generated, here, we use $n = 1000$.

For each realisation, the measurement in each channel is a linear mixture of typical values of each surface type, weighted by the the area fraction of each surface type. This is solved for the area

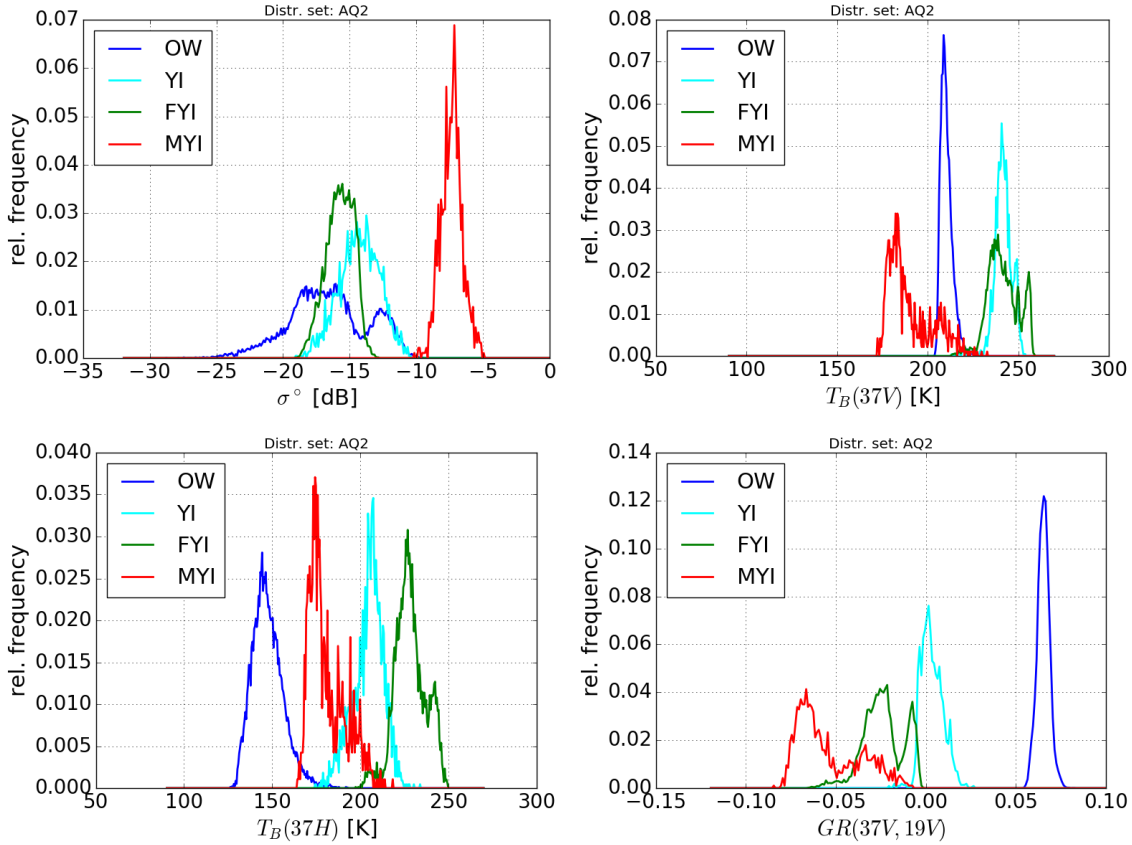

Figure 2: *Distribution of ASCAT σ^0 (top left), AMSR2 T_B at 36.5* GHz, *V polarisation (top right); AMSR2 T_B at 36.5* GHz, *H polarisation (bottom left), and AMSR2 GR(37V,19V) (bottom right) for three* ***Antarctic*** *sea ice types MYI (red), FYI (green), YI (light blue) and for open water (blue).*

fractions under the constraints that the area fractions must add up to one and that each area fraction must be between 0 and 1 (constrained optimisation problem).
Then the median of the n solutions for the area fractions is the final result. Note that the area fractions of the different ice types are usually called *concentrations*.
In addition, the spread of the n solutions around the median is a measure of confidence of the result for each surface type. Normalised to the interval 0..1, this is saved as confidence level.
Note that since we do not use the 89 GHz channel, we do not use the ECICE weather filters. We use, however, an additional open-water filter, using the gradient ratios of 37 and 19 GHz, V polarisation, and 22 and 19 GHz, V polarisation: a pixel is considered 100% open water if

$$GR_{37V,19V} < 0.05 \text{ and } GR_{22V,19V} < 0.024 \tag{2}$$

3.2 Coast correction

Directly at a coast, the signal of the scatterometer or radiometer can contain contribution from the land (“land contamination”), resulting in erroneous high MYI concentration in pixels directly at the coast in the Arctic. This can lead to large errors later in the season, in particular along the Northeastern Siberian coast. Therefore, during the first 10 days of the season retrieved (end of

Parameter	Meaning	Value	Note
T_1	thresh. temp., start of warm episode	-1°C	Arctic & Antarctic
T_2	thresh. temp., end of warm episode	2°C	Arctic & Antarctic
N	max. duration of warm episode	10 days	Arctic & Antarctic
ΔC_t	min. drop of MYI conc.	10%	Arctic & Antarctic

Table 2: *Parameter setting for the* ***temperature correction*** *scheme*

September), a zone that is one pixel wide, along all coasts of Eurasia is cleared of MYI unless connected to MYI offshore. This is done before applying the correction schemes. Note that in the Canadian Archipelago, sea ice can persist along coasts, in particular in channels between islands. Therefore, the coast correction is not applied there. Moreover, the coast correction is not being applied in the Antarctic at all.

3.3 Correction Schemes

The determination of the ice type concentrations (i.e., the area fractions of the three ice types) is only based on their radiometric and backscattering properties. Surface melting and refreezing, snow wetness, snow metamorphosis in particular at temperatures close to melting, and other processes such as deformation can cause erroneous sea ice type concentrations. Such errors are reduced by the two corrections schemes.

3.3.1 Temperature Correction

Warm episodes, caused by warm air advection, can occur in particular during the transition seasons. When temperatures rise to near melting or beyond melting conditions, MYI can temporarily look like FYI for the ECICE algorithm, so it is misclassified as FYI (more precisely: the retrieved MYI is too low and the FYI concentration too high). After the end of the warm event, the ice is again correctly classified. In order to correct for that, the temperature correction scheme Ye et al. (2016a) looks, in T2m data, for episodes of up to N days that start with temperatures rising above a threshold T_1 (near freezing temperature) and that end with temperatures falling below a threshold of T_2. If at the same time at the location of the warm episode, the MYI concentration first drops by more than ΔC_t and later rises again, such MYI concentrations are replaced by values linearly interpolated from before and after the warm episode. The values for N, T_1, T_2, ΔC_t are given in Table 2.

3.3.2 Drift Correction

The drift correction (Ye et al., 2016b) prevents erroneous MYI seemingly generated during the freezing season. MYI starts by definition as all remaining ice at the end of the melting season, i.e., at freeze-up. After that, it can only drift and be changed by divergence, convergence, and melting, but can not be generated. Therefore, we construct a domain around the MYI of the preceding day where the MYI could have drifted in one day. This is done by applying the ice motion vector for one day to all pixels inside areas of nonzero MYI concentration. This domain is then further extended by one grid cell to the outside. Any MYI that has been retrieved outside if this domain cannot be multiyear ice. Therefore, all nonzero MYI concentrations in grid cells outside the mentioned domain are set to zero. However, since this spurious/erroneous MYI is in fact FYI or YI that has special radiometric and scattering properties (because to ECICE, it looked like MYI), it is kept

Parameter	Meaning	Value	Note
ΔC_d	min. rise of MYI conc.	20%	Arctic & Antarctic
ΔT_{37}	min. drop of $T_{B,37H}$	20 K	Arctic & Antarctic
ΔT_{19-37}	min. drop of $T_{B,19H}$-$T_{B,37H}$	10 K	Arctic & Antarctic

Table 3: *Parameter setting for the* ***drift correction*** *scheme*

as a new pseudo-ice-type, which we call Ex-MYI. In addition, this correction scheme includes correction for some effects of snow metamorphosis: It looks for sudden (within one day) rises ΔC_d of MYI concentration concurrent with sudden reductions ΔT_{37} of $T_{B,37H}$ or with reductions ΔT_{19-37} of $T_{B,19H} - T_{B,37H}$. In such cases, the MYI concentration is replaced by the value of the previous day. The threshold values ΔC_d, ΔT_{19-37}, and $T_{B,19H}$ are given in Table 3.

3.4 Gridding

All swath data of AMSR-E or AMSR2 brightness temperatures of one calendar day (with respect to UTC) are resampled (gridded) into a polar stereographic grid using the routine *nearneighbor* of the software package *Generic Mapping Tools* (*GMT*), version 5.2.1. This means that we use daily gridded brightness temperatures, not swath data as input.
The ASCAT data are also gridded to the same grid, likewise, the sea ice motion data and the temperature data.
For both hemispheres, we use the standard Arctic and Antarctic polar stereographic grids of the National Snow and Ice Data Center (NSIDC) at 12.5 km grid spacing (about the grids, see https://nsidc.org/data/polar-stereo/ps_grids.html). The EPSG code[3] is 3411 for the Arctic and 3412 for the Antarctic grid. An overview of the two regions and the grids is in Table 4

Region	Grid	grid spacing	parameters	size (pixels)
Arctic	NSIDC North	12.5 km	std lat:70°N,std lon: 45°W	608 × 896
Antarctic	NSIDC South	12.5 km	std lat:70°S,std lon: 0°	632 × 664

Table 4: *Hemispheric regions and their polar stereographic map projection properties. Note; "std lat" is standard latitude of the projection, "std lon" its standard longitude; "size (pixels)" is x-coordinate (number of columns) by y-coordinate (number of rows).*

4 Verification/Validation

The corrected MYI concentration for the Arctic has been tested and verified by comparison with high-resolution synthetic aperture radar (SAR), see details in Ye et al. (2016b); Ye (2016). The corrected MYI concentration for the Antarctic has been verified against high-resolution SAR images, charts of sea ice "stage of development" jointly provided by the U.S. National Ice Center (NIC) and by the Russian Arctic and Antarctic Research Institute (AARI) (http://ice.aari.aq/antice/); the maps of YI concentration have been compared with a satellite-based data set of Antarctic polynya/thin ice data (method based on Kern et al., 2007). Further validation studies are planned in 2019 and 2020.

[3] See http://www.epsg-registry.org/

5 Product Description

The product, i.e. the initial uncorrected ice type concentrations ("raw ice types") as well as the corrected MYI concentration ("final product") comes in various formats (detail below):

- NetCDF file containing the gridded ice concentration data
- image files (PNG) showing maps of sea ice type concentrations

Data access is via HTTP or FTP, see https://seaice.uni-bremen.de. The archive directory structure and file naming is best explained by an example:
Intermediate data:
`data/MultiYearIce/ascat-amsr2/raw/Antarctic/png/2017/`
`ECICE-IcetypesUncorrected-20170911-MYI.png`
Final data:
`data/MultiYearIce/ascat-amsr2/final/Antarctic/png/2017/`
`MultiYearIce-Antarctic-20170911.png`
where

ascat : Scatterometer; currently only `ascat`

amsr2 : Radiometer; `amsr2` or `amsre`

raw : branch, either intermediate data `raw` or final data `final`

Antarctic : Hemisphere; `Arctic` or `Antarctic`

png : Format, either `png` for map images or `netcdf` for NetCDF data

2017 : Year

ECICE- : Prefix for intermediate data which are direct output of ECICE

20170591 : Year, month and day in the format `YYYYMMDD`

-MYI : The intermediate data maps have a suffix for the ice type; in NetCDF format all three ice types are contained in one file, so not suffix is needed

5.1 NetCDF

The NetCDF files contains 2-dimensional fields, gridded in the polar-stereographic grids at 12.5 km grid spacing. They also contain the needed projection and grid information and are GIS compatible. The intermediate result files contain the following variables (arrays of the same dimensions):

- Latitude and longitude
- six possible input channels: ASCAT σ^0 (`BKAS`), AMSR2 $T_{B,19H}$, $T_{B,37H}$, $T_{B,37V}$, $GR_{37V,19V}$, $GR_{22V,19V}$
- MYI, FYI, YI and total ice concentrations, open water concentration
- the confidence levels for each sea ice type concentration

The final result files contain the following variables (arrays of the same dimensions):

- corrected MYI concentration (`MYI`)
- Ex-MYI concentration(`EXMYI`)
- flag indicating which correction type was done by the drift correction (`CR-FLAG`)

5.2 Maps

The maps are produced adding coast lines, land and geographic grid lines to the ice type concentration data. Example maps of one day with uncorrected ice types and final MYI shown in Figure 3. Note that the maps are not meant for quantitative data analysis.

6 Caveats, retrieval problems

While the final MYI data retrieved from active and passive microwave data and corrected using temperature and ice drift data are considerably more realistic than data retrieved simply from radiometer data, some problems still remain:
Weather influence on the surface of the MYI (including the snow cover) can cause considerable day-to-day fluctuation of MYI concentration - a moving average or several days might reduce them, but is currently not applied. In the Eastern Arctic (Kara and Laptev Sea), unrealistically high MYI concentrations occur in March, April and May. They are probably caused by small areas of spurious MYI caused by rough young ice (possibly with wet snow). In the Antarctic, a similar phenomenon, i.e., unrealistically high MYI in the Northern Ross Sea and West of it in late winter and spring, is probably caused by grounded icebergs. The intermediate data, of course, have not been corrected for surface processes at all, therefore they have to be taken with caution, they are provided as is. We are grateful of any feedback on unexpected features and possible problems of the data.

A AMSR-E and AMSR2 swath data

A.1 AMSR-E

AMSR-E Level 1A data, version 3, are used (see Section 2 above). They contain raw observation counts and calibration parameters that are read and converted to brightness temperatures according to the documentation of the data (Japan Aerospace Exploration Agency (JAXA), 2009, see also https://nsidc.org/data/amsrel1a/versions/3/documentation). In addition, the data contain the geolocation information for each footprint. The geolocation information is then corrected following the approach by Wiebe et al. (2008).

A.2 AMSR2

AMSR2 Level 1B, version 2.220.220 are used (see Section 2 above). They contain the calibrated brightness temperatures and the geolocation information. The ECICE algorithm and the correction schemes haves been developed and validated for the Arctic with AMSR-E brightness temperatures Ye et al. (2016a,b) The successor instrument AMSR2 has similar, but not identical channels and

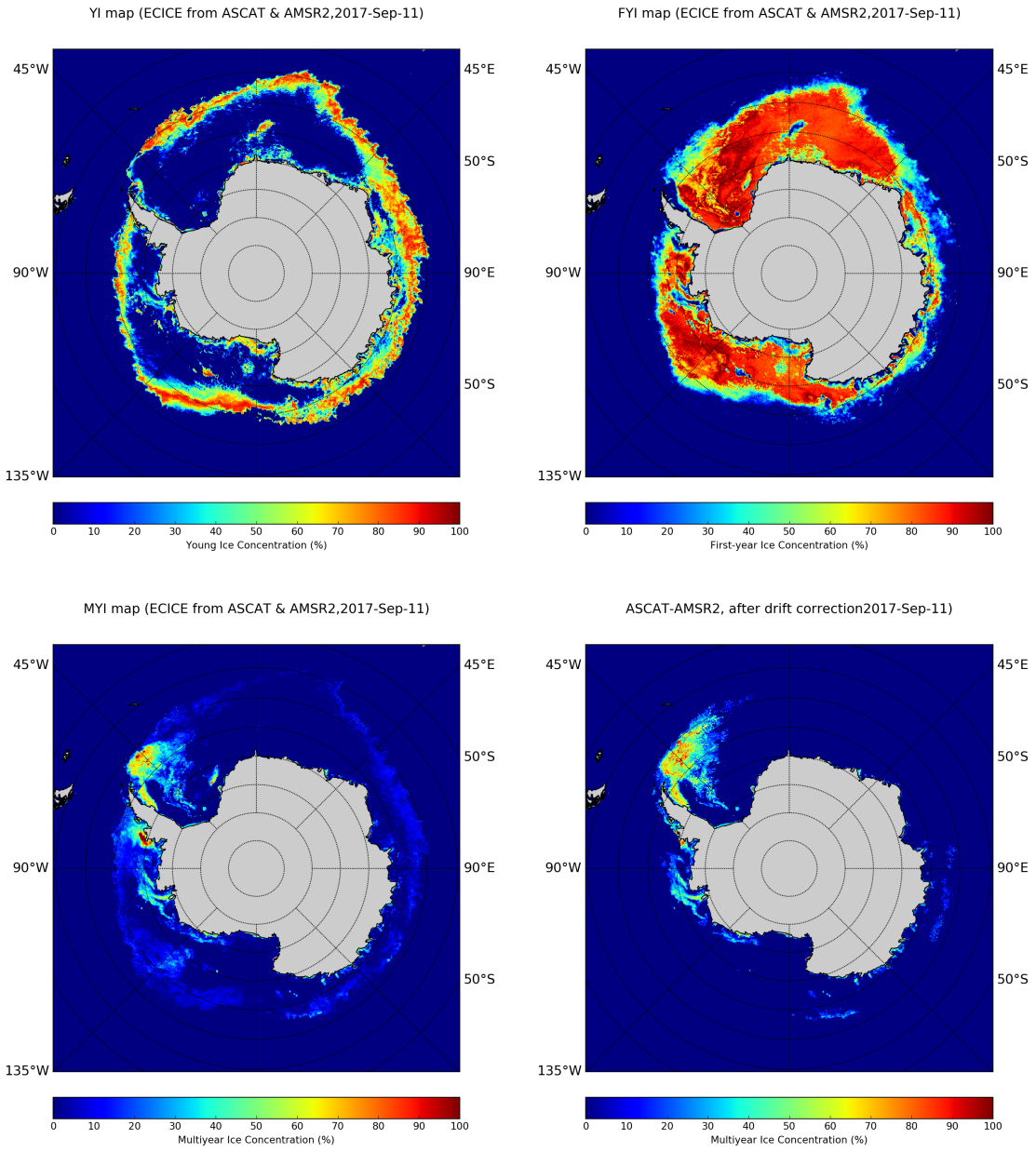

Figure 3: *Intermediate product (output from ECICE) and final product (corrected MYI) of the IUP MYI processing chain, for 11 Sept., 2017. Top left: uncorrected YI concentration; top right: uncorrected FYI concentration; bottom left: uncorrected MYI concentration; bottom right: corrected MYI concentration.*

channel characteristics. A regression analysis of co-located AMSR-E and AMSR2 data[4] yields coefficients for converting AMSR2 brightness temperatures into equivalent AMSR-E brightness temperatures, so the original ASI algorithm for AMSR-E can be applied. The set of coefficients

[4] Although the scanning mechanism of the AMSR-E antenna reflector broke down in October 2011, the antenna still measured brightness temperatures well into the lifetime of AMSR2

used here is given in Section B.

B Coefficients for conversion of AMSR2 T_bs to AMSR-E T_bs

The intercalibration coefficients between AMSR2 and AMSR-E brightness temperatures were derived by a linear regression of the differences between AMSR-E and AMSR2 brightness temperatures, ascending and descending swaths combined,

$$T_{B,\mathrm{AMSR2}} - T_{B,\mathrm{AMSR-E}} = s\,T_{B,AMSR2} + i \tag{3}$$

The resulting slope s and intercept i, taken from JAXA (2015) and, for the 89 GHz A scan channels and the 7 GHz channel, from Okuyama and Imaoka (2015), are listed in Table 5. So in order to

Channel	Slope s	Intercept i
6V	-0.01390	3.67421
6H	-0.00940	3.03663
7V	-0.00567	2.66603
7H	-0.00702	3.13950
10V	-0.01289	6.34775
10H	-0.00221	3.79624
18V	-0.04524	12.57562
18H	-0.00858	1.89574
23V	-0.00957	4.40435
23H	-0.00947	4.18710
36V	-0.01019	5.49799
36H	-0.00985	4.19181
89V, A scan	-0.01488	5.65119
89H, A scan	-0.04014	12.36275
89V, B scan	-0.01403	5.32379
89H, B scan	-0.00980	3.75174

Table 5: *Coefficient for linear conversion of AMSR2 to AMSR-2 brightness temperatures, from the second intercalibration (JAXA (2015)). Values for the 7* GHz *channels and for the 89* GHz *A-scan channels were taken from the first intercalibration (Okuyama and Imaoka, 2015).*

convert AMSR2 brightness temperatures to AMSR-E brightness temperatures, we have to apply

$$T_{B,\mathrm{AMSR-E}} = (1-s)T_{B,\mathrm{AMSR2}} - i \tag{4}$$

References

Japan Aerospace Exploration Agency (JAXA). AMSR-E/Aqua L1A Raw Observation Counts, Version 3. NASA National Snow and Ice Data Center Distributed Active Archive Center, Boulder, Colorado. https://doi.org/10.5067/AMSR-E/AMSREL1A.003, 2003, updated daily. Accessed: September 2018.

Japan Aerospace Exploration Agency (JAXA). *Aqua AMSR-E Level 1 Product Format Description Document*, 2009. URL https://nsidc.org/sites/nsidc.org/files/files/data/amsre/amsr-e_format_l1_e.pdf.

Japan Aerospace Exploration Agency (JAXA). Intercomparison results between AMSR2 and TMI/AMSR -E/GMI (AMSR2 Version 2.0). JAXA, https://suzaku.eorc.jaxa.jp/GCOM_W/materials/product/150326_AMSR2_XcalResults.pdf, March 2015. Accessed: October 2018.

S. Kern, G. Spreen, L. Kaleschke, S. De La Rosa, and G. Heygster. Polynya Signature Simulation Method polynya area in comparison to AMSR-E 89GHz sea-ice concentrations in the Ross Sea and off the Adélie coast, antarctica, for 2002: first results. *Annals of Glaciology*, 46:409–418, 2007. doi: 10.3189/172756407782871585.

T. Lavergne, S. Eastwood, Z. Teffah, H. Schyberg, and L.-A. Breivik. Sea ice motion from low resolution satellite sensors: an alternative method and its validation in the arctic. *Journal of Geophysical Research*, 115:C10032, 2010. doi: 10.1029/2009JC005958.

T. Okuyama and K. Imaoka. Intercalibration of Advanced Microwave Scanning Radiometer-2 (AMSR2) brightness temperature. *IEEE Transactions on Geoscience Remote Sensing*, 55(8): 4568 – 4577, August 2015. doi: 10.1109/TGRS.2015.2402204.

M. Shokr and T. A. Agnew. Validation and potential applications of Environment Canada Ice Concentration Extractor (ECICE) algorithm to arctic ice by combining AMSR-E and QuikSCAT observations. *Remote Sensing of Environment*, 128:315–332, 2013. ISSN 0034-4257. doi: 10.1016/j.rse.2012.10.016. URL http://www.sciencedirect.com/science/article/pii/S003442571200404X.

M. Shokr, A. Lambe, and T. Agnew. A new algorithm (ECICE) to estimate ice concentration from remote sensing observations: An application to 85-GHz passive microwave data. *IEEE Transactions on Geoscience Remote Sensing*, 46(12):4104–4121, dec 2008. doi: 10.1109/tgrs.2008.2000624.

M. Tschudi, C. Fowler, J. Maslanik, J. S. Stewart, and W. Meier. Polar Pathfinder daily 25 km EASE-Grid sea ice motion vectors, Version 3. (Arctic, Antarctic). NASA National Snow and Ice Data Center Distributed Active Archive Center. Boulder, Colorado USA, 2016. URL https://nsidc.org/data/nsidc-0116/versions/3. doi: 10.5067/O57VAIT2AYYY.

H. Wiebe, G. Heygster, and L. Meyer-Lerbs. Geolocation of AMSR-E data. *IEEE Transactions on Geoscience Remote Sensing*, 46(10):3098–3103, 2008. doi: 10.1109/TGRS.2008.919272.

Y. Ye. *Correcting Multiyear Sea Ice Concentration Estimates from Microwave Satellite Observations with Air Temperature, Sea Ice Drift and Dynamic Tie Points*. PhD thesis, University of Bremen, Germany, 2016.

Y. Ye, G. Heygster, and M. Shokr. Improving multiyear ice concentration estimates with reanalysis air temperatures. *IEEE Transactions on Geoscience Remote Sensing*, 54(5):2602–2614, 2016a. doi: 10.1109/tgrs.2015.2503884.

Y. Ye, M. Shokr, G. Heygster, and G. Spreen. Improving multiyear sea ice concentration estimates with sea ice drift. *Remote Sensing*, 8(5):397, 2016b. doi: 10.3390/rs8050397.